Electron states in a GaAs quantum dot in a magnetic field

Arvind Kumar
*IBM Research Division, Thomas J. Watson Research Center, P.O. Box 218, Yorktown Heights, New York 10598 and Department of Electrical Engineering and Computer Science, Massachusetts Institute of Technology, Cambridge, Massachusetts 02139**

Steven E. Laux and Frank Stern
IBM Research Division, Thomas J. Watson Research Center, P.O. Box 218, Yorktown Heights, New York 10598
(Received 12 March 1990; revised manuscript received 6 June 1990)

Self-consistent numerical solutions of the Poisson and Schrödinger equations have been obtained for electron states in a GaAs/$Al_xGa_{1-x}As$ heterostructure with confinement in all three spatial dimensions. The equations are solved in the Hartree approximation, omitting exchange and correlation effects. Potential profiles, energy levels, and the charge in the quantum dot are obtained as functions of the applied gate voltage and magnetic field. First, the zero-magnetic-field case is considered, and the quantum-dot charge is allowed to vary continuously as the gate voltage is swept. Then, in connection with the phenomenon of Coulomb blockade, the number of electrons in the quantum dot is constrained to integer values. Finally, the calculation is extended to examine the evolution of levels in a magnetic field applied perpendicular to the heterojunction. Our results indicate that the confining potential has nearly circular symmetry despite the square geometry of the gate, that the energy levels are quite insensitive to the charge in the quantum dot at a fixed gate voltage, and that the evolution of levels with increasing magnetic field is similar to that found for a parabolic potential.

I. INTRODUCTION

Modern fabrication techniques have made possible confinement of a two-dimensional layer of electrons into wires, grids, or dots where quantum-mechanical effects are strongly manifested. Of particular current interest are quasi-zero-dimensional systems, which have been made by selective etching of a GaAs cap on a GaAs-$Al_xGa_{1-x}As$ heterostructure,[1] by depositing a cross-grid gate structure on a GaAs heterostructure[2] or on Si,[3] by using crossed holographically defined gratings,[4] and by using an array of small Latex particles as an etch mask,[5] to cite some recent examples. Such quantum-dot structures offer a dispersionless system with an electron-energy spectrum that can be modulated either by varying gate bias voltage or by applying an external magnetic field. Smith *et al.*[1] have reported oscillatory structure in capacitance versus gate voltage in zero magnetic field and have attributed it to the discrete energy states of a quantum dot. Recently, Hansen *et al.*[6] have reported observing Zeeman splitting of quantum-dot capacitance features, as expected when a magnetic field is applied perpendicular to the heterojunction. There are many papers that treat the energy-level structure of related systems, including the paper by Darwin that treats a two-dimensional harmonic-oscillator potential in the presence of a normal magnetic field,[7] Robnik's paper on a disk in a magnetic field,[8] and the recent calculations by Brum and co-authors on a model quantum dot.[6,9] Sivan and Imry[10] have described the evolution of states in a quantum dot versus magnetic field in relation to magnetization and persistent currents, which are not considered here. In this paper we present numerical self-consistent results in the Hartree approximation for potential profiles, energy levels, envelope wave functions, and charge distributions for quantum dots like those studied by Hansen *et al.*[6]

Self-consistent numerical treatments of electron states in quasi-one-dimensional systems in the absence of a magnetic field have been carried out for a narrow channel in silicon by Laux and Stern[11] and for a split-gate GaAs/$Al_xGa_{1-x}As$ heterostructure by Laux *et al.*[12] Numerical methods for such systems, which have quantities that vary in two spatial dimensions, have also been used by Kojima *et al.*[13] and by Kerkhoven *et al.*[14] However, the analogous calculation for a totally confined system requires a coupled solution of Poisson's equation and Schrödinger's equation in three spatial dimensions, increasing the computation requirements significantly. Application of a magnetic field, which leads to complex wave functions and a Hermitian rather than a real symmetric eigenvalue problem, also adds to the computational burden. In Sec. II we discuss our formulation of this problem. In Sec. III we discuss results of such a calculation on a GaAs/$Al_xGa_{1-x}As$ quantum-dot structure in zero applied magnetic field. In particular, we discuss the effect of varying the charge in the quantum dot on the energy-level structure and the quasi-Fermi-level, and its relation to the Coulomb blockade.[15]

In Sec. IV we extend our self-consistent calculation to include the effect of an applied magnetic field perpendicular to the heterojunction on the potential, charge density, and electron states of the quantum dot. We find good

qualitative agreement with the results of earlier calculations for model potentials.

II. FORMULATION OF THE PROBLEM

The structure we consider is a model of a single quantum dot from the array of dots used in the experiments of Hansen *et al.*,[6] described above. It is based on a heterostructure with an n-type GaAs substrate layer with a net ionized donor concentration of 10^{18} cm^{-3}, an 80-nm layer of undoped GaAs (a background acceptor concentration of 10^{14} cm^{-3} is assumed throughout and diffusion of donors from the substrate is ignored), a 20-nm layer of undoped $Al_{0.4}Ga_{0.6}As$, a 20-nm layer of the same material with a donor concentration of 1.5×10^{18} cm^{-3}, and a 30-nm GaAs cap layer. The cap is etched away, except in the central 300 nm$\times$300 nm portion of a 500 nm$\times$500 nm area, and the structure repeats on a square lattice. Finally, a metal gate is deposited over the entire top surface. A negative voltage on the gate depletes the charges in the GaAs channel, except under the remaining GaAs cap, and this three-dimensionally confined "puddle" of electrons is the quantum dot being studied. The n-type GaAs substrate allows a low-impedance capacitative contact to the dot. Figure 1 shows the conduction-band edge in the structure versus vertical distance along a line through the center of the dot, and in the inset is sketched the semiconductor region included in the model.

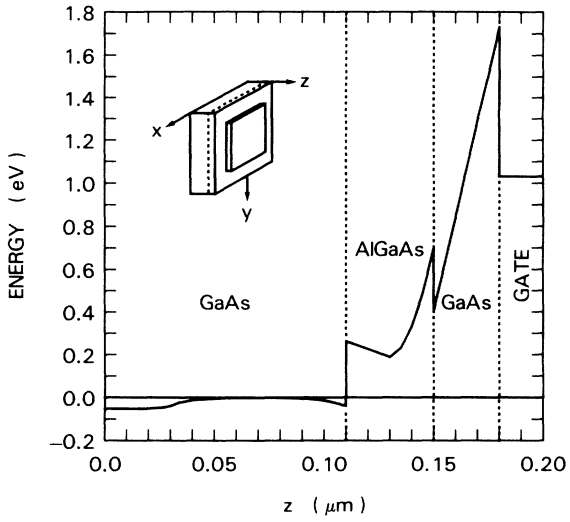

FIG. 1. Conduction-band edge along a vertical line through the center of the GaAs-$Al_xGa_{1-x}As$ structure considered here, for a gate voltage of -1.03 V. The layers of the structure, from left to right, are 30 nm of n^+-GaAs, 80 nm of undoped GaAs, 20 nm of undoped $Al_{0.4}Ga_{0.6}As$, 20 nm of $Al_{0.4}Ga_{0.6}As$ with $N_D=1.5\times10^{18}$ cm^{-3}, and a 30 nm GaAs cap. The repeating unit is 500 nm square, and the GaAs cap layer is etched away, except under a central 300-nm square mesa. A metallic gate is then deposited over the structure. The Schottky barrier associated with the gate suppresses induced charge in the GaAs, except under the central portion of the mesa. All calculated results are for 4.2 K and the zero of energy is taken at the Fermi level in the substrate.

For the GaAs, we use an electron effective mass of $0.07m_0$ and a dielectric constant of 13; for the $Al_xGa_{1-x}As$, we use $0.11m_0$ and 11.8, respectively, corresponding to an AlAs mole fraction $x=0.4$. The conduction-band offset is taken to be 0.3 eV. The binding energy of the deep donor in the $Al_{0.4}Ga_{0.6}As$ is taken to be 0.15 eV, and the effective Schottky-barrier heights of the gate electrode to the GaAs and the $Al_{0.4}Ga_{0.6}As$ are taken to be 0.7 and 0.95 eV, respectively.

Although the present calculations deal with the structure of Hansen *et al.*,[6] the methods to be described in this paper can be used for a wide class of structures in which three-dimensional confinement of electrons is achieved by a combination of band offsets and electrostatic means.

We solve the Schrödinger and Poisson equations self-consistently. Image effects[16] in the Schrödinger equation are ignored and we use the Hartree approximation, ignoring exchange and correlation effects. Bryant[17] showed that many-electron interactions can have significant quantitative and qualitative influence on the energy spectrum of a quantum dot with a small number of electrons. Similar effects are expected for the structures studied here, but have not been included in our calculation.

The electrostatic potential ϕ is governed by the Poisson equation

$$\nabla\cdot[\epsilon(x,y,z)\nabla\phi(x,y,z)]=-\rho(x,y,z)\ , \tag{1}$$

where ϵ is the permittivity (in the present case it depends only on the z coordinate), with boundary conditions determined by voltages applied at the contacts. At boundaries where there are no contacts, the normal derivative of the potential is taken to be zero. The total charge density ρ in Eq. (1) includes the charge in quantum states, calculated as described below, as well as the contribution from ionized impurities in the $Al_xGa_{1-x}As$, and of any electrons outside the Schrödinger domain. In particular, any electrons in the cap layer are treated classically.

In a magnetic field (B_x,B_y,B_z) the three-dimensional Schrödinger equation for the electron envelope function (in the effective-mass approximation) becomes

$$\sum_{j=1}^{3}\left[\frac{\hbar}{i}\frac{\partial}{\partial x_j}+eA_j\right]\frac{1}{2m_j}\left[\frac{\hbar}{i}\frac{\partial}{\partial x_j}+eA_j\right]\zeta_n +[U(x,y,z)-E_n]\zeta_n=0\ , \tag{2}$$

where m_j is the electron effective mass in the jth direction and the electron charge is $-e$. We choose the symmetric gauge

$$A_x=(B_yz-B_zy)/2\ , \tag{3}$$

and cyclic permutations. In the present case $m_x=m_y=m_z$ and $B_x=B_y=0$.

The electron charge density in the quantum dot is

$$\rho_{\rm inv}(x,y,z)=-2e\sum_n\zeta_n^*(x,y,z)\zeta_n(x,y,z) \times f((E_{qF}-E_n)/k_BT))\ , \tag{4}$$

where the sum is over all states n, the factor 2 is for spin degeneracy (spin splitting is ignored in this calculation), E_{qF} is the quasi-Fermi-energy, and f is the Fermi-Dirac occupation function at temperature T.

If the Fermi energy in the quantum dot is equal to the Fermi energy in the n-type substrate, then the calculated charge in the dot will be a continuous function of the gate voltage. The charge per quantum dot will, in general, be a nonintegral multiple of the electron charge, and will represent the average for a large ensemble of dots. Physically, however, the charge in an isolated dot should be an integral multiple of the electron charge. If we constrain the charge in the dot to be an integral multiple of the electron charge, then we apply Fermi-Dirac statistics to determine the quasi-Fermi-level that gives the prescribed charge from the calculated energy levels.

Among many simplifying assumptions in our calculation is the neglect of the interface image potential and of many-electron contributions to the potential. Then the potential energy is $U=-e\phi+\Delta E_c$, where the second term is the position-dependent conduction-band offset relative to the bottom of the conduction band in the GaAs. Level broadening has not been included explicitly, but some broadening, small compared to typical level spacings, is simulated because we carry out the calculations at $T=4.2$ K.

Both the Poisson and Schrödinger equations are cast into discrete form on a nonuniformly graded, tensor-product (finite-difference) mesh, with no interior mesh-line terminations,[18] and the resultant matrix equations are solved numerically. The Schrödinger mesh includes only the region of significant dot charge; elsewhere electrons are treated semiclassically. Electrostatic potential, envelope functions, and charge-density values are defined at mesh nodes, whereas material properties such as dielectric constant, effective mass, and effective band-edge shift ΔE_c are piecewise constant in the individual rectangular parallelepiped elements defined by the mesh. Equations for the potential and envelope function at each node are obtained by integrating Eqs. (1) and (2) over the box defined by the six planes bisecting the lines connecting the node to its nearest neighbors (for nodes on the boundary, only the volume inside the boundary is included). For the Poisson equation, this results in a real symmetric matrix problem $\bar{\mathbf{L}}\boldsymbol{\phi}=-\boldsymbol{\Omega}\boldsymbol{\rho}$, where $\bar{\mathbf{L}}$ is the operator $\nabla\cdot\epsilon\nabla$ integrated over the boxes, $\boldsymbol{\phi}$ and $\boldsymbol{\rho}$ are vectors of the nodal potentials and charge densities, and $\boldsymbol{\Omega}$ is a diagonal matrix of the nodal box volumes. For the Schrödinger equation, one similarly obtains $\bar{\mathbf{H}}\boldsymbol{\zeta}_n=E_n\boldsymbol{\Omega}\boldsymbol{\zeta}_n$, where $\bar{\mathbf{H}}$ is the Hamiltonian integrated over the boxes and $\boldsymbol{\zeta}_n$ is the complex vector of the envelope function for state n at each node. This equation is readily transformed into a standard matrix eigenvalue problem by premultiplying both sides by $\boldsymbol{\Omega}^{-1/2}$ and substituting $\mathbf{I}=\boldsymbol{\Omega}^{-1/2}\boldsymbol{\Omega}^{1/2}$ to give $(\boldsymbol{\Omega}^{-1/2}\bar{\mathbf{H}}\boldsymbol{\Omega}^{-1/2})(\boldsymbol{\Omega}^{1/2}\boldsymbol{\zeta}_n)=E_n(\boldsymbol{\Omega}^{1/2}\boldsymbol{\zeta}_n)$, or simply $\mathbf{H}\mathbf{y}_n=E_n\mathbf{y}_n$, where $\mathbf{H}=\boldsymbol{\Omega}^{-1/2}\bar{\mathbf{H}}\boldsymbol{\Omega}^{-1/2}$ is still an Hermitian matrix and $\mathbf{y}_n=\boldsymbol{\Omega}^{1/2}\boldsymbol{\zeta}_n$. In zero magnetic field, the Hermitian matrix reverts to a real symmetric matrix.

The Poisson equation in discrete form is nonlinear, since the charge density depends on the potential. The solution to this nonlinear problem constitutes the search for self-consistency between the charge and the potential. The solution to the Schrödinger equation enters as part of the evaluation of the total charge density in the device, for a given potential. We linearize the Poisson equation via Newton's method. The vector $\boldsymbol{\phi}$ which is the zero of the function $\mathbf{F}(\boldsymbol{\phi})=\bar{\mathbf{L}}\boldsymbol{\phi}+\boldsymbol{\Omega}\boldsymbol{\rho}(\boldsymbol{\phi})$ is sought by iterating

$$\mathbf{F}'(\boldsymbol{\phi}^l)\tilde{\boldsymbol{\phi}}^l=-\mathbf{F}(\boldsymbol{\phi}^l)\ , \tag{5a}$$

$$\boldsymbol{\phi}^{l+1}=\boldsymbol{\phi}^l+t\tilde{\boldsymbol{\phi}}^l\ , \tag{5b}$$

until convergence is obtained. Here, l is the iteration index and the scalar damping factor t is selected according to a modified Bank-Rose damping scheme as discussed in Ref. 19. The evaluation of the Jacobian matrix $\mathbf{F}'$ is a possible stumbling block because the dependence on $\boldsymbol{\phi}$ of the charge density in the channel given in Eq. (4) is nonlocal, which would destroy the seven-diagonal structure of the Jacobian, rendering the matrix solution significantly more difficult. Instead, as discussed in Ref. 19, a rather crude approximation to the dependence of the channel charge on local potential is made for purposes of calculating $\mathbf{F}'$ only, in order to circumvent this difficulty. While this precludes a second-order convergence rate of the Newton iteration, converged solutions can still be obtained in an acceptable number of iterations. The linear matrix equations in (5a) above are solved via a conjugate-gradient method. Such methods require a preconditioner to accelerate convergence; we have selected a polynomial preconditioner,[20] as it has proven robust and highly vectorizable.

The discrete Schrödinger equation is solved by one of two methods. Far away from self-consistency between charge and potential, a Lanczos method is employed.[21] This method forms an approximate tridiagonalization $\mathbf{T}$ of the matrix $\mathbf{H}$. No reorthogonalization is used in this process. Then, the eigenvalues of $\mathbf{T}$ are found in a specified energy interval (from the minimum of the quantum dot potential to 5–10 meV above the Fermi energy) by a bisection search together with Sturm sequencing.[21] Care must be taken in discarding potentially "spurious" eigenvalues of $\mathbf{T}$, that is, eigenvalues of $\mathbf{T}$ which are not good approximations to true eigenvalues of $\mathbf{H}$.[21] Finally, inverse iteration is used to find the associated eigenvectors. Gaussian elimination is used to solve the tridiagonal matrix equations involved in inverse iteration.

Near self-consistency between the charge and the potential, a simple Rayleigh quotient-iteration algorithm[22] is used to solve the eigensystem. This algorithm requires an initial guess for the eigenfunctions, and can be summarized as follows. Let $\sigma(\mathbf{y})=(\mathbf{y}^H\mathbf{H}\mathbf{y})/(\mathbf{y}^H\mathbf{y})$ be the usual Rayleigh quotient (superscript H denotes Hermitian conjugate) and let $\mathbf{y}^0$ be an initial guess for the nth eigenfunction. Then solve

$$[\mathbf{H}-\sigma(\mathbf{y}^l)\mathbf{I}]\mathbf{x}^{l+1}=\mathbf{y}^l\ , \tag{6a}$$

$$\mathbf{y}^{l+1}=\mathbf{x}^{l+1}/\|\mathbf{x}^{l+1}\|\ , \tag{6b}$$

$$\mathbf{y}^{l+1}=\mathbf{y}^{l+1}-\sum_{i=0}^{n-1}(\mathbf{y}_i^H\mathbf{y}^{l+1})\mathbf{y}_i \quad \text{(this step only if } n>0)\ ; \tag{6c}$$

$$\text{if } \|\mathbf{H}\mathbf{y}^{l+1}-\sigma(\mathbf{y}^{l+1})\mathbf{y}^{l+1}\| < \epsilon, \quad \text{then done .} \tag{6d}$$

The solution becomes $\mathbf{y}_n = \mathbf{y}^{l+1}$ and $E_n = \sigma(\mathbf{y}^{l+1})$.

Note that the step (6c) above is not a part of the standard Rayleigh quotient iteration. This step serves to remove components related to previously determined eigenfunctions $\mathbf{y}_i$, $i = 0, 1, 2, \ldots, n-1$, from the vector $\mathbf{y}^{l+1}$ which is evolving into the eigenfunction $\mathbf{y}_n$. In practice, this orthogonalization step has an important benefit: In solving the equations for a series of gate voltages or magnetic fields, the time-consuming Lanczos method can be omitted from the iteration for self-consistency between charge and potential, provided the new solution is not too distant from the previous solution. The orthogonalization ensures that energy levels which are "close" at some initial solution do not converge to the same level at a later step. This procedure gives correct eigenstates using significantly less computation time, but may eventually miss some intermediate eigenvalues if extended over too wide a range of gate voltage or magnetic field without an intervening Lanczos solution.

The Hermitian matrix system in (6a) above is solved with the polynomial-preconditioned conjugate-gradient method.[20] Although the matrix $\mathbf{H}-\sigma\mathbf{I}$ in (6a) is not positive definite, this method of solution has always been robust for the class of problems we have encountered.

The boundary condition used in our numerical method is that the normal derivative of ζ_n vanish on the Schrödinger mesh boundary. In the lateral (x and y) directions this condition occurs sufficiently far from the region of induced charge that it has no appreciable effect on the results. In the direction normal to the inversion layer, we truncate the Schrödinger mesh 36 nm below the GaAs/Al_xGa_{1-x}As interface to avoid the quasicontinuum of eigenstates arising from the heavily n-type doped substrate. This may lead to significant errors in the values of energy levels and thresholds. In particular, some of the qualitative results for the present structure may not apply to a dot with stronger vertical confinement, as could be obtained if a p-type substrate were used.

The convergence criterion for self-consistency is that the nodal potential energies of successive iterations differ by no more than 0.01 meV anywhere on the Poisson mesh. The necessarily limited mesh size ($51\times51\times35$ for the Poisson mesh and $43\times43\times18$ for the Schrödinger mesh, in the x, y, and z directions, respectively) and other approximations made in the calculation will lead to errors that are larger than this convergence criterion. An IBM 3090 computer with vector processor was used for these calculations. A single Newton's loop, in which the Poisson and Schrödinger equations are each solved once, required approximately 15 min of computation time for $B=0$ and 45 min for $B\neq0$ if the Lanczos recursion was used. If the Rayleigh quotient algorithm was used in place of the Lanczos method, the solution of the Schrödinger equation (nearly all the computation time) ranged from 5 to 50 times faster, depending on the quality of the initial guess. A typical bias point required 4–20 Newton's loops to converge.

III. ZERO MAGNETIC FIELD

Potential contours in a plane 8 nm below the GaAs-Al_xGa_{1-x}As interface, near the maximum of the electron charge distribution, are shown in Fig. 2. Note that the potential contours are nearly circular, especially at the lower energies, although the defining gate geometry is a square. That follows from the attenuation of higher Fourier components of the potential in regions some distance from the gate, as found previously for fluctuations in the width of a gate opening.[23] Also, the effective size of the quantum dot, given by the contour at the Fermi level, is considerably smaller than the size of the defining structure in the gate. In Fig. 2 and throughout this paper we make cuts in representative planes or along representative lines to display functions of three spatial coordinates. The figures are intended to indicate the main features of the calculated results, but should not be considered to be complete. The raggedness of some of the later curves is a consequence of the necessarily coarse mesh used in the discretization.

Figure 3 shows the number of electrons in the quantum dot, the lowest-energy levels, and the quasi-Fermi-level as functions of the voltage on the gate at 4.2 K for zero magnetic field. The notion of "quasi-Fermi-level" does not arise in calculations for quasi-one-dimensional wires, for which the charge can be considered to vary continuously, provided a suitable means of equilibrating with an adjacent gate or contact exists. For the very small structures considered here, where a dot may contain only a

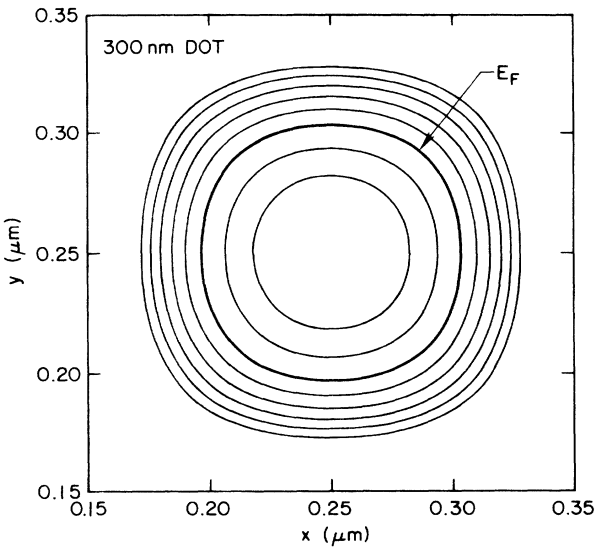

FIG. 2. Lateral potential contours in the plane 8 nm below the GaAs/Al_xGa_{1-x}As interface, near the peak of the vertical charge density, for a gate voltage of -1.03 V. The innermost contour is 15 meV below the Fermi level, which is indicated by the heavy line, and the remaining contours are at 10-meV intervals from -10 to $+50$ meV. Note the nearly circular symmetry despite the square geometry of the cap. The effective quantum dot size, with a diameter of about 100 nm, is considerably smaller than the 300-nm square mesa in the GaAs cap layer.

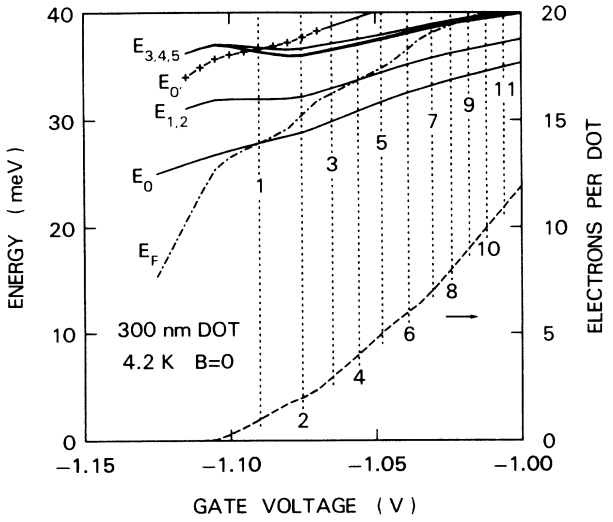

FIG. 3. Energy levels (solid lines) and Fermi level (dotted-dashed line) relative to the bottom of the potential well, and number of electrons in the quantum dot (dashed line), vs gate voltage. The second level is doubly degenerate, and the next three levels lie very close to each other. In addition, each level has a twofold spin degeneracy. These energies reflect the combined effect of vertical and lateral confinement. The energy of the lowest state with a node in the z direction is indicated by the plus signs. Only integer electron occupations, indicated by the vertical dotted lines, correspond to physically realizable states of an isolated quantum dot.

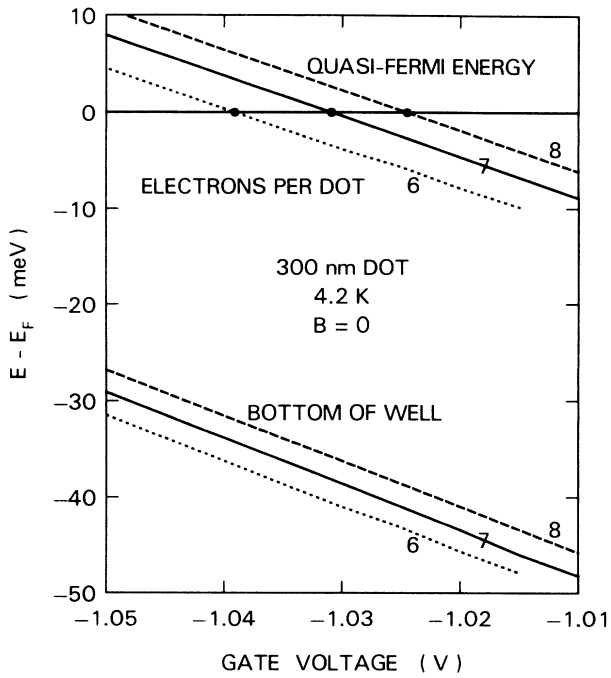

FIG. 4. Quasi-Fermi-level and energy of the bottom of the well, vs gate voltage for six, seven, and eight electrons in the quantum dot. The energy difference between the quasi-Fermi-level and the Fermi level gives a driving force for electrons to move between the dot and the substrate. The circles correspond to gate voltages for which the dot is in equilibrium with the substrate for an integer electron occupation.

few electrons, discontinuities can arise because transfer of just one electron can have a significant effect on the energies in the problem. This gives rise to the Coulomb blockade, as found in many experiments.[15] Because of this effect, the curves in Fig. 3 have no physical signficance for an isolated quantum dot at points where the number of electrons in the dot is different from an integer.

Some of the energy levels we calculate are degenerate (apart from the spin degeneracy, which applies to all levels in our calculation) and others are nearly so. For example, the second and third levels are exactly degenerate at zero magnetic field because of the square symmetry of the structure we consider. The fourth and fifth levels would be degenerate at $B=0$ if our system had circular symmetry. The small splitting results from the weak remnant of the square symmetry of the cap. Finally, the sixth level, which is close to the fourth and fifth, would be exactly degenerate with them if the system had circular symmetry and had the perfectly parabolic potential treated by Darwin.[7] Similar considerations apply for higher-lying levels, except that they are increasingly influenced by the deviations from a circularly symmetric potential.

Figure 4 shows the quasi-Fermi-energy and the bottom of the potential relative to the Fermi energy in the GaAs substrate when the number of electrons in the quantum dot is six, seven, or eight. At a given gate voltage, several different charge states of the dot are possible, although the state with the quasi-Fermi-level closest to the Fermi level in the substrate contact is the one most likely to be observed. The buildup of potential difference before a charge transfer occurs is a signal of the Coulomb blockade.[15]

One measure of capacitance of our structure is obtained by using the lower curve in Fig. 3 to calculate a gate-to-dot capacitance $C_g = dQ_{\rm QD}/dV_g$. That capacitance varies from about 1×10^{-17} F at small values of dot charge to about 3×10^{-17} F when there are about 12 electrons per dot. More directly relevant to the experiment of Hansen *et al.*[6] is an effective substrate-to-dot capacitance C_s, which we obtain by dividing the electron charge by the vertical separation between successive quasi-Fermi-level curves in Fig. 4, to obtain a value of about 6×10^{-17} F for a dot occupation between seven and eight electrons. Both of these effective capacitances will increase with increasing dot charge.

The dynamical behavior of this system depends on charge-transfer rates between the quantum dot and adjacent electrodes, a problem which is outside the scope of the present static calculation.[15] Note that the barrier between the dot and the substrate is very small, as indicated in Fig. 1 for a line through the center of the dot. This barrier would have been larger had we used a larger value than 10^{14} cm^{-3} for the net acceptor doping in the nominally undoped GaAs.

Figure 5 shows a few of the lowest-energy levels versus gate voltage when the number of electrons in the quan-

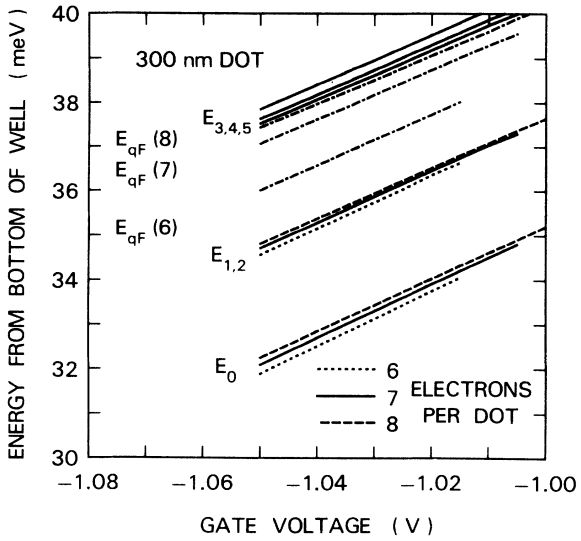

FIG. 5. The six lowest-energy levels (note that the second and third levels are degenerate), and the quasi-Fermi-energies, for six, seven, and eight electrons per quantum dot, vs gate voltage. Each level has a twofold spin degeneracy. For the upper three levels only the values for seven electrons per dot are shown; the results for six and eight electrons per dot almost coincide. These results are for 4.2 K and $B=0$.

tum dot is fixed at six, seven, or eight with zero magnetic field. The energy levels depend remarkably little on the charge state, but are quite sensitive to gate voltage.

Some details of potential and charge density are given in Figs. 6–8, both as functions of charge in the quantum dot at $B=0$ and as functions of magnetic field (as discussed in the next section) for fixed charge in the dot. Figure 6 shows the charge density along a vertical line through the center of the dot. The charge density peaks about 8 nm below the $GaAs/Al_xGa_{1-x}As$ interface, but is truncated—as described above—before the rise of charge density in the substrate begins. A lateral cut through the charge density near the peak in Fig. 6 is shown in Fig. 7. Finally, Fig. 8 shows the variation of the conduction-band edge in the x direction, in the same plane as in Fig. 7. The effective size of the dot is about 100 nm, considerably smaller than the 300-nm square mesa in the GaAs cap layer. The potential somewhat resembles the truncated parabola found previously for n-i-p-i doping superlattices[24] and for wires in Si (Ref. 11) and GaAs,[12] but with more structure, which can be attributed to the small number of discrete states that contribute to the charge in the cases shown.

IV. NONZERO MAGNETIC FIELDS

When a magnetic field is applied normal to the surface, the Schrödinger equation, Eq. (2), becomes complex, and

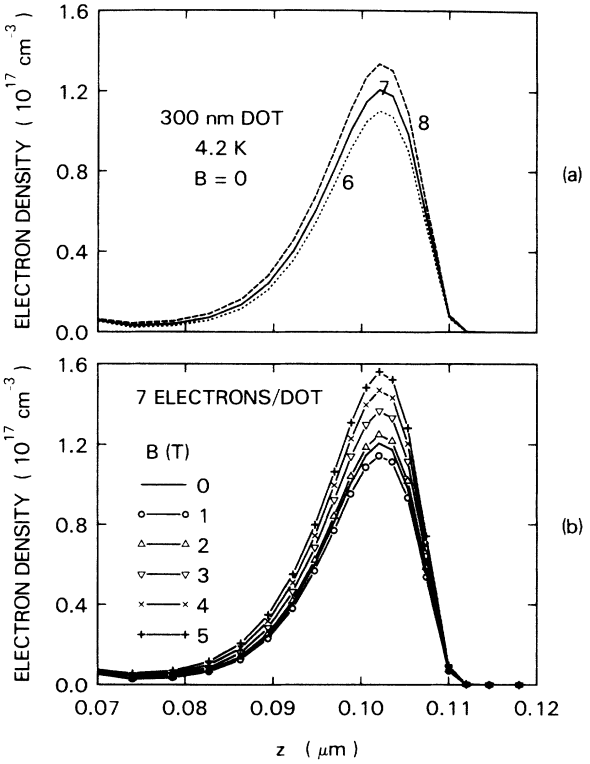

FIG. 6. Total charge density in the vertical direction along a line through the quantum dot center for (a) six, seven, and eight electrons per dot, with $B=0$, and (b) $B=0$, 1, 2, 3, 4, and 5 T, with seven electrons per dot. The z coordinate and the gate voltage are the same as in Fig. 1.

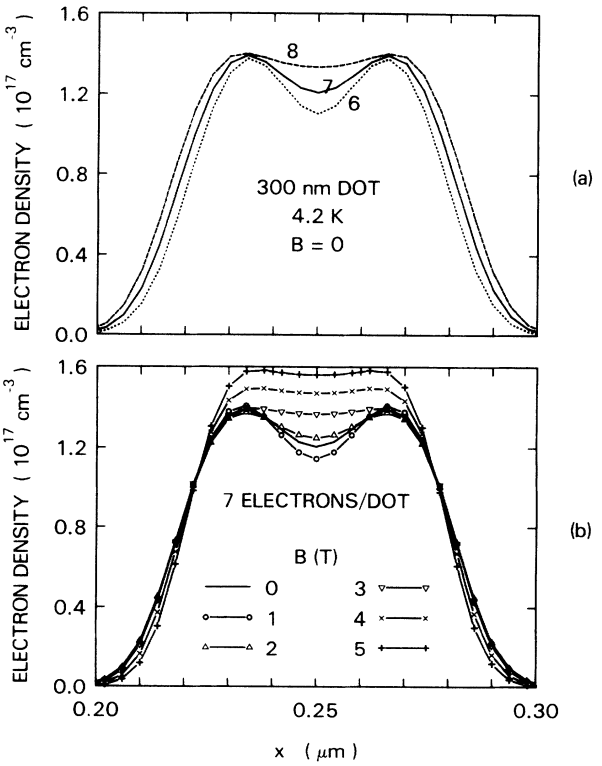

FIG. 7. Lateral cut of total charge density in a plane 8 nm below the $GaAs/Al_xGa_{1-x}As$ interface. The cut is taken through the center of the quantum dot. Other quantities as in Fig. 6.

TABLE I. Calculated quantities for states of the quantum dot at 4.2 K for $B=5$ T and a gate voltage of -1.03 V, with seven electrons in the dot. The energy is relative to the bottom of the potential well in the dot, $\langle l_z \rangle$ is the expectation value of the z component of the "canonical" angular momentum $\mathbf{r}\times\mathbf{p}$, $\langle R \rangle$ is the expectation value of the two-dimensional radial distance from a vertical axis through the center of the dot, δR is its standard deviation, and $\langle L_z \rangle$ is the expectation value of the z component of the total angular momentum $\mathbf{r}\times m\mathbf{v}$. The 0′ state is the lowest state with a node in the z direction.

State	Energy (meV)	$\langle l_z \rangle/\hbar$	$\langle R \rangle$ (nm)	δR (nm)	$\langle L_z \rangle/\hbar$
0	35.4	0.07	14.3	7.5	1.06
1	35.5	−1.05	21.2	7.5	0.87
2	35.7	−1.98	25.9	7.3	0.76
3	36.2	−2.91	29.4	7.1	0.57
4	37.0	−3.83	32.3	6.9	0.32
5	38.1	−4.75	34.8	6.8	0.03
6	39.5	−5.62	37.1	6.6	−0.24
7	41.1	−6.46	39.1	6.6	−0.49
8	42.9	−7.32	41.0	6.5	−0.78
9	43.6	0.98	21.0	7.4	2.87
0′	43.7	0.00	15.9	9.4	1.30

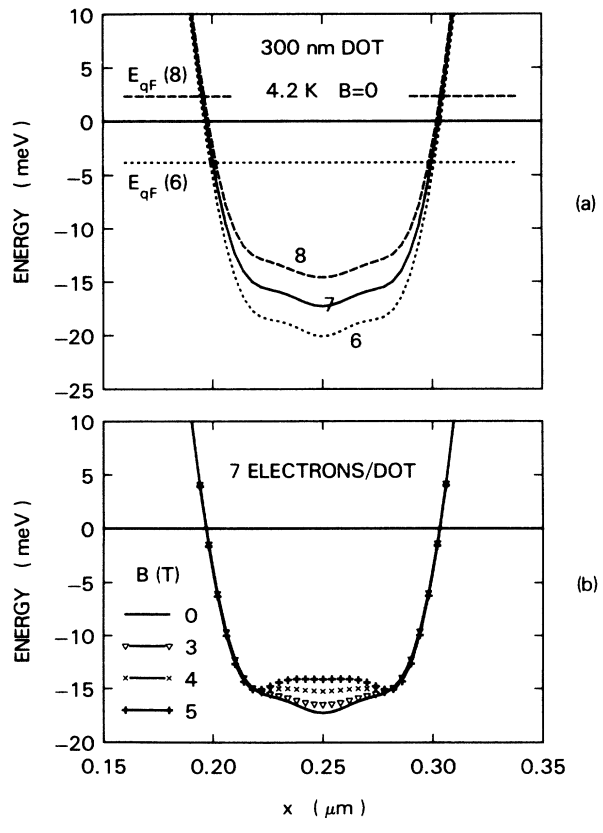

FIG. 8. Potentials along the same line as in Fig. 7. The Fermi energy is at zero. The quasi-Fermi-energies for six and eight electrons per quantum dot are indicated in (a). The quasi-Fermi-energy is within 1 meV of the Fermi energy for seven electrons per dot for the range of magnetic fields shown, and has been omitted. Also omitted in (b) are the curves for $B=1$ and 2 T, which lie very close to the curve for $B=0$.

its discretized form leads to an Hermitian matrix. In our case, this matrix has about 30 000 rows and columns, and a corresponding number of eigenstates, but we typically look for only the ~20 eigenstates with the lowest energy. Nevertheless the calculation, as described above, is very time consuming. We show in Fig. 9 the energy levels for the case of seven electrons per quantum dot, with a gate

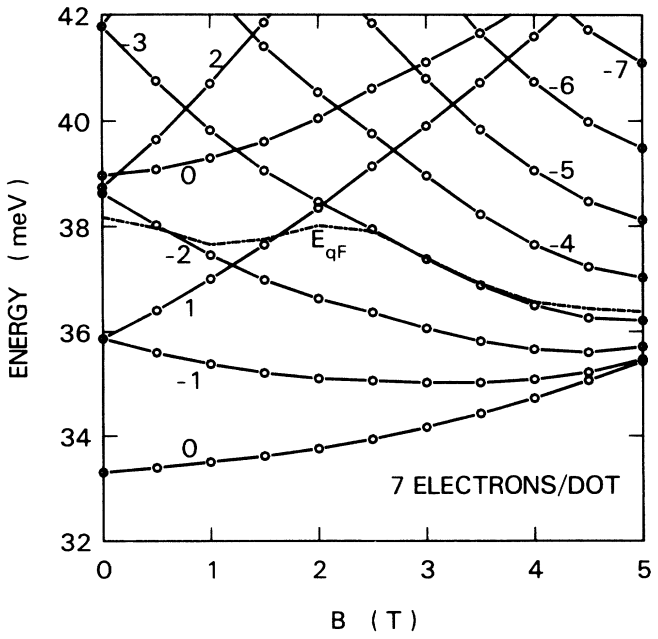

FIG. 9. Energy levels vs magnetic field for a quantum dot with seven electrons and a gate voltage of -1.03 V. The labels give *approximate* values of the z component of the canonical angular momentum $\mathbf{r}\times\mathbf{p}$ in units of $\hbar$.

voltage of -1.03 V. As shown in Fig. 2, the potential has nearly circular symmetry, and therefore angular momentum is approximately a good quantum number. The curves are labeled with an integer to represent the approximate z component of angular momentum (in units of $\hbar$), but the calculated expectation values for the points shown differ from an integer by up to 10%, and by less than 0.1 for the zero-angular-momentum states. These labels should therefore be considered to have only qualitative significance. At $B=0$, where the envelope eigenfunctions are real, the angular momentum is zero for all the states. The calculated curves are in good qualitative agreement with the results found by Darwin[7] for states in a two-dimensional harmonic-oscillator potential in a magnetic field. The curves are shown to cross, as would apply for states with different angular momentum in a circularly symmetric potential, although we expect that small anticrossing gaps would appear if the calculation were carried out with greater resolution. The difference between the crossing behavior in a circularly symmetric case and the anticrossing for positive-parity states in a rectangular box is nicely illustrated in Figs. 1 and 2 of the paper by Robnik.[8]

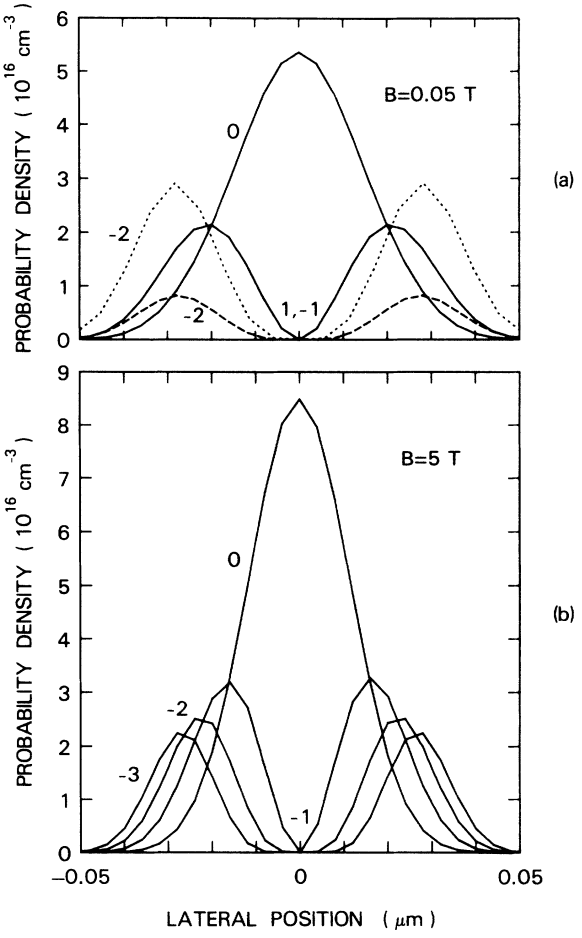

FIG. 10. Probability densities (absolute squares of the normalized envelope wave functions) for the four lowest eigenstates, in a plane 8 nm below the GaAs/$Al_xGa_{1-x}As$ interface. The gate voltage is -1.03 V and there are seven electrons in a quantum dot. Results are shown for (a) $B=0.05$ T and (b) $B=5$ T. The labels give the *approximate* value of the z component of the canonical angular momentum in units of $\hbar$. The states labeled $1,-1$ for $B=0.05$ T have probability densities which are almost the same (they correspond to opposite angular-momentum combinations of the x- and y-like degenerate solutions for $B=0$). The probability densities for the states shown in both (a) and (b) are approximately circularly symmetric, except for the state labeled -2 in (a), for which cuts along the x direction (dashed line) and along the diagonal $x=y$ (dotted line) are shown.

The angular momentum referred to in the preceding paragraph is what Van Vleck[25] has called the canonical angular momentum. It is the expectation value of $\mathbf{l}=\mathbf{r}\times\mathbf{p}$, where $\mathbf{p}$ is the operator $-i\hbar\nabla$. The "true" angular momentum, $\mathbf{L}=\mathbf{r}\times m\mathbf{v}$, has an additional term[25,26] $(e/2)\mathbf{r}\times(\mathbf{B}\times\mathbf{r})$, analogous to the additional term in the Hamiltonian in the presence of a magnetic field. The angular-momentum quantum number associated with the z component of the canonical angular momentum is the integer l that appears in the angular factor $\exp(il\phi)$ in the wave function in a circularly symmetric potential.

Table I gives some additional information for the lowest states for $B=5$ T. We show the expectation value of the energy relative to the bottom of the well, of the z component of the canonical angular momentum, of $R=(x^2+y^2)^{1/2}$, with lateral position measured relative to a vertical axis through the center of the quantum dot, of $\delta R=(\langle R^2\rangle-\langle R\rangle^2)^{1/2}$, and of the z component of the "true" angular momentum, $\langle L_z\rangle=\langle l_z\rangle+(eB/2)\langle R^2\rangle$. The last state in the table is the lowest state with a node in the z direction.

The expectation value of the true angular momentum for a one-electron problem is related to the magnetic moment μ by[25] $\mu_z=-dE/dB=-(e/2m)\langle L_z\rangle$, where we assume the magnetic field to be in the z direction, as in the example treated in this paper. Our numerical results deviate somewhat from this relation, a difference which we attribute to the inclusion of the Hartree terms for the electron-electron interaction in the potential energy.

The energy levels in Fig. 9 are all associated with states that have no nodes in the z direction. States with such nodes, which would correspond to the first excited subband in a two-dimensional electron gas in an unpatterned GaAs heterojunction, appear at energies above 42 meV.

As already shown in Figs. 6–8, the character of the solution changes with increasing magnetic field. The radial wings of the charge density contract, with a corresponding increase in charge density near the center of the quantum dot and a change in the shape of the bottom of the potential well. The shape of the charge density of the four lowest states in a dot with seven electrons is shown in Fig. 10 for magnetic fields of 0.05 and 5 T. Even at 5 T, for which the magnetic length, $(\hbar/eB)^{1/2}=11$ nm, is considerably smaller than the effective dot radius, about 50 nm, a distinction between bulklike and edgelike states is not obvious from the charge densities or angular momenta of the occupied states. Note that spin splittings, which we have ignored, will become significant at the upper end of the magnetic field range that we use.

V. DISCUSSION

As noted earlier, many approximations have been made in these calculations. In particular, the substrate structure of the sample we have modeled required truncation of the Schrödinger mesh on a plane where the wave functions had not yet decayed to zero. There must be another, for the present not well understood, approximation in our description of the sample, because the calculated voltage threshold is about -1 V, while the measured threshold is about -0.2 V.[6] The measurements are made in the dark, and the calculations use a deep-donor binding energy consistent with that condition. The large discrepancy between calculated and measured threshold voltages may be due to changes in the properties of the top layers and of the interfaces caused by the processing steps used in defining the lateral sample geometry. The neglect of many-body interactions is also significant. We expect, however, that many of the qualitative results for the internal structure of the quantum dot remain valid.

We found that the energy-level structure can be considered to be a perturbation of the states of a parabolic potential in a magnetic field, with angular momentum a rough guide to the properties of the states. We also found, in contrast to our original expectations, that the energy levels measured from the bottom of the potential well are quite insensitive to the number of electrons in the quantum dot, for a fixed gate voltage. A weak dependence of level separations on electron population was obtained theoretically by Chaplik.[27] A number of authors have found theoretically that optical transitions for a parabolic potential in superlattices,[28] quantum wells,[29] wires,[30] and dots[31] reflect the underlying structure of the bare harmonic-oscillator potential and are unaffected by electron-electron interactions. Experiments on quantum wires[32] and quantum dots[2,4] are consistent with this result.

We have shown how the quasi-Fermi-level in the quantum dot depends on gate voltage for different charge states of the dot. As the gate voltage changes from a value corresponding to an integer electron occupation, the difference between the quasi-Fermi-level in the dot and in the adjacent substrate electrode increases, related to the Coulomb blockade. The gate voltage at which the charge changes discretely is not considered here. Finally, we gave some pictures of energy levels and wave functions, with approximate values of angular momentum, for a range of values of gate voltage, charge in the dot, and magnetic field.

At least one of the authors began this work expecting to find a clear qualitative distinction between bulklike and edgelike states. Our computed envelope wave functions do not show any abrupt qualitative differences, which can be considered to be a consequence of the rather soft potential at the walls of the quantum dot.

Note added in proof. Since completion of this work we have become aware of two related publications. The eigenfunctions and eigenvalues of the two-dimensional harmonic oscillator in a magnetic field were obtained by Fock[33] three years before the paper by Darwin.[7] Maksym and Chakraborty[34] have treated the energy levels of quantum dots with three and four electrons moving in a two-dimensional harmonic oscillator potential with an applied magnetic field, including effects of electron-electron interaction.

ACKNOWLEDGMENTS

We are indebted to Ralph Willoughby and Jane Cullum for access to the Lanczos eigenvalue program used here, to Mark Amidon, Len Borucki, Orest Bula, Steve Furkay, and Fred Pileggi for graphics and database support in earlier stages of our work, to Trey Smith for information about the samples and for discussions of the experiments and their interpretation, to Jose Brum for discussions of his calculations, and to Boris Alt'shuler, Pradip Bakshi, Gottfried Döhler, Alan Fowler, Wolfgang Hansen, Joe Imry, Khalid Ismail, Rolf Landauer, Uri Sivan, and Phil Stiles for helpful discussions and comments.

---

*Present address.

[1]T. P. Smith III, K. Y. Lee, C. M. Knoedler, J. M. Hong, and D. P. Kern, Phys. Rev. B **38**, 2172 (1988).

[2]C. T. Liu, K. Nakamura, D. C. Tsui, K. Ismail, D. A. Antoniadis, and H. I. Smith, Appl. Phys. Lett. **55**, 168 (1989).

[3]J. Alsmeier, E. Batke, and J. P. Kotthaus, Phys. Rev. B **41**, 1699 (1990).

[4]U. Sikorski and Ch. Merkt, Phys. Rev. Lett. **62**, 2164 (1989).

[5]H. Fang, R. Zeller, and P. J. Stiles, Appl. Phys. Lett. **55**, 1433 (1989).

[6]W. Hansen, T. P. Smith III, K. Y. Lee, J. A. Brum, C. Knoedler, D. Kern, and J. M. Hong, Phys. Rev. Lett. **62**, 2168 (1989).

[7]C. G. Darwin, Proc. Cambridge Philos. Soc. **27**, 86 (1931).

[8]M. Robnik, J. Phys. A **19**, 3619 (1986).

[9]J. A. Brum and G. Bastard, in *Science and Engineering of One- and Zero-Dimensional Semiconductors*, edited by S. P. Beaumont and C. M. Sotomayor-Torres (Plenum, New York, in press).

[10]U. Sivan and Y. Imry, Phys. Rev. Lett. **61**, 1001 (1988).

[11]S. E. Laux and F. Stern, Appl. Phys. Lett. **49**, 91 (1986).

[12]S. E. Laux, D. J. Frank, and F. Stern, Surf. Sci. **196**, 101 (1988).

[13]K. Kojima, K. Mitsunaga, and K. Kyuma, Appl. Phys. Lett. **55**, 882 (1989).

[14]T. Kerkhoven, A. T. Galick, J. H. Arends, U. Ravaioli, and Y. Asad, J. Appl. Phys. (to be published).

[15]See, for example, R. Wilkins, E. Ben-Jacob, and R. C. Jaklevic, Phys. Rev. Lett. **63**, 801 (1989), and references therein to earlier work.

[16]The image potential associated with the different dielectric constants of GaAs and $Al_xGa_{1-x}As$ has been shown to have a very small effect on energy levels in a heterojunction [F. Stern and S. Das Sarma, Phys. Rev. B **30**, 840 (1984)] and is expected to have an insignificant effect on the results of the present calculation.

[17]G. Bryant, Phys. Rev. Lett. **59**, 1140 (1987).

[18]See, for example, G. E. Forsythe and W. R. Wasow, *Finite*

Difference Methods for Partial Differential Equations (Wiley, New York, 1960).

[19]S. E. Laux, in *Proceedings of the Fifth International Conference on the Numerical Analysis of Semiconductor Devices and Integrated Circuits (NASECODE V)*, edited by J. J. H. Miller (Boole, Dun Laoghaire, Ireland, 1987), pp. 270–275.

[20]O. G. Johnson, C. A Micchelli, and G. Paul, SIAM J. Numer. Anal. **20**, 362 (1983).

[21]J. K. Cullum and R. A. Willoughby, *Lanczos Algorithms for Large Symmetric Eigenvalue Computations* (Birkhäuser, Boston, 1985), Vols. I *(Theory)* and II *(Programs)*.

[22]B. N. Parlett, *The Symmetric Eigenvalue Problem* (Prentice-Hall, Englewood Cliffs, NJ, 1980).

[23]A. Kumar, S. E. Laux, and F. Stern, Appl. Phys. Lett. **54**, 1270 (1989).

[24]P. Ruden and G. H. Döhler, Phys. Rev. B **27**, 3538 (1983).

[25]J. H. Van Vleck, *The Theory of Electric and Magnetic Susceptibilities* (Oxford University Press, London, 1932), Secs. 7 and 36.

[26]H. L. Zhao, Y. Zhu, and S. Feng, Phys. Rev. B **40**, 8107 (1989).

[27]A. V. Chaplik, Pis'ma Zh. Eksp. Teor. Fiz. **50**, 38 (1989) [JETP Lett. **50**, 44 (1989)].

[28]P. Ruden and G. H. Döhler, Phys. Rev. B **27**, 3547 (1983).

[29]L. Brey, N. F. Johnson, and B. I. Halperin, Phys. Rev. B **40**, 10 647 (1989).

[30]V. B. Shikin, T. Demel, and D. Heitmann, Zh. Eksp. Teor. Fiz. **96**, 1406 (1989) [Sov. Phys.—JETP **69**, 797 (1989)].

[31]K. Kempa, D. A. Broido, and P. Bakshi, Bull. Am. Phys. Soc. **35**, 768 (1990); P. Bakshi, D. A. Broido, and K. Kempa, Phys. Rev. B (to be published).

[32]W. Hansen, M. Horst, J. P. Kotthaus, U. Merkt, Ch. Sikorski, and K. Ploog, Phys. Rev. Lett. **58**, 2586 (1987).

[33]V. Fock, Z. Phys. **47**, 446 (1928).

[34]P. A. Maksym and T. Chakraborty, Phys. Rev. Lett. **65**, 108 (1990).